Exchange Coupling and Energy-Level Crossing in a Magnetic Chain $[Dy_2Cu_2]_n$ Evaluated by High-Frequency Electron Paramagnetic Resonance

Atsushi Okazawa,[†,‡] Takashi Nogami,[†] Hiroyuki Nojiri,*[,§] and Takayuki Ishida*[,†,‡]

Department of Applied Physics and Chemistry and Course of Coherent Optical Science, The University of Electro-Communications, Chofu, Tokyo 182-8585, Japan, and Institute for Materials Research, Tohoku University, Katahira, Sendai, Miyagi 980-8577, Japan

Received December 11, 2007. Revised Manuscript Received February 16, 2008

A 4f−3d heterometallic polymeric coordination compound $[\{Dy(hfac)_2(CH_3OH)\}_2\{Cu(dmg)(Hdmg)\}_2]_n$ ($[Dy_2Cu_2]_n$; H_2dmg = dimethylglyoxime; Hhfac = 1,1,1,5,5,5-hexafluoropentane-2,4-dione) was synthesized, and the X-ray crystallographic analysis shows that the structure is isomorphous to the known ferrimagnetic $[Gd_2Cu_2]_n$ polymer. A centrosymmetric diamond-arrayed ferrimagnetic unit involving the oximate bridge, Dy−O−N−Cu, is repeated to form a discrete chain. An onset of the frequency dependence was found in the ac magnetic susceptibility measurements down to 1.8 K. Low-temperature magnetization measurements on $[Dy_2Cu_2]_n$ exhibited magnetic hysteresis with magnetization steps. To examine the energy level structure and the exchange coupling between the Dy and Cu ions, high-frequency EPR (HF-EPR) spectra of a polycrystalline sample of $[Dy_2Cu_2]_n$ were recorded at various frequencies (34.7−525.4 GHz) and temperatures. We analyzed the spectra by treating the Dy moments as Ising spins and built an exchange-coupling model for a diamond-arrayed tetranuclear macrocycle $[Dy_2Cu_2]$. The Dy−Cu exchange couplings were precisely evaluated, owing to the high resolution of HF-EPR; J/k_B = −0.895(8) and −0.061(8) K for two independent Dy−Cu relations, where the exchange parameter is defined as $-J$. The Cu···Cu coupling among the macrocycles was estimated to be ferromagnetic with approximately 1 K. The present study has established the definitive methodology to examine the energy level in 4f−3d heterometallic systems by using HF-EPR. The magnetic properties of the $[Dy_2Cu_2]_n$ chain were plausibly described as a perturbed system of a single-molecule magnet. The quantum tunneling of the magnetization is based on a different principle compared with those of the 3d-based single-molecule magnets, since the energy level structure of $[Dy_2Cu_2]_n$ is regulated by the exchange couplings.

Introduction

Low-dimensional coordination compounds with bridging ligands are of increasing interest for development of molecule-based magnets since the discovery of single-molecule magnets (SMMs) and related systems such as single-chain magnets (SCMs).[1–4] We have employed a strategy using oximate coordination compounds for a nonserendipitous synthesis of oligo-nucleating compounds, since the N−O groups are versatile to bridge in heterometallic systems.[4,5] Actually, a variety of compounds have been rationally synthesized such as the linear trinuclear [DyCuDy] complex using 2,2′-dipyridyl ketoximate[6] and centrosymmetric pentanuclear complex [Dy_4Cu] bridged by dianionic dimethylglyoximate (dmg^{2-}).[7] Distinct SMM behaviors are found in those compounds, and moreover, the exchange couplings have been evaluated based on an Ising model. Such quantitative analysis is quite rare but an essential ingredient of the systematic research of molecule-based magnets including lanthanide ions. The next direction may be the synthesis of one-dimensional compounds, and in fact much effort has been paid to metal−radical alternating coordination compounds[8–10] and heterometallic chain compounds,[4,11] for example. We have also applied the dmg-bridging architecture to 4f−3d heterometallic SCMs and have successfully obtained the $[Gd_2Cu_2]_n$ ferrimagnetic chain.[12] Along this line,

* To whom correspondence should be addressed. Tel: +81-42-443-5490. Fax: +81-42-443-5501 (T.I.). E-mail: ishi@pc.uec.ac.jp (T.I.); nojiri@imr.tohoku.ac.jp (H.N.).
† Department of Applied Physic and Chemistry, UEC.
‡ Course of Coherent Optical Science, UEC.
§ Tohoku University.

(1) Gatteschi, D.; Sessoli, R.; Villain, J. *Molecular Nanomagnets*; Oxford, University Press Inc.: New York, 2006.
(2) Sessoli, R.; Gatteschi, D. *Angew. Chem., Int. Ed.* **2003**, *42*, 268.
(3) Christou, G.; Gatteschi, D.; Hendrickson, D. N.; Sessoli, R. *MRS Bull.* **2000**, *25*, 66.
(4) Clérac, R.; Miyasaka, H.; Yamashita, M.; Coulon, C. *J. Am. Chem. Soc.* **2002**, *124*, 12837.
(5) Lloret, F.; Ruiz, R.; Cervera, B.; Castro, I.; Julve, M.; Faus, J.; Real, J. A.; Sapiña, F.; Journaux, Y.; Colin, J. C.; Verdaguer, M. *J. Chem. Soc., Chem. Commun.* **1994**, 2615.
(6) Mori, F.; Nyui, T.; Ishida, T.; Nogami, T.; Choi, K.-Y.; Nojiri, H. *J. Am. Chem. Soc.* **2006**, *128*, 1440.
(7) Ueki, S.; Ishida, T.; Nogami, T.; Choi, K.-Y.; Nojiri, H. *Chem. Phys. Lett.* **2007**, *440*, 263.
(8) Caneschi, A.; Gatteschi, D.; Lalioti, N.; Sangregorio, C.; Sessoli, R.; Venturi, G.; Vindigni, A.; Rettori, A.; Pini, M. G.; Novak, M. A. *Angew. Chem., Int. Ed.* **2001**, *40*, 1760.
(9) Miyasaka, H.; Madanbashi, T.; Sugimoto, K.; Nakazawa, Y.; Wernsdorfer, W.; Sugiura, K.-I.; Yamashita, M.; Coulon, C.; Clérac, R. *Chem. Eur. J.* **2006**, *12*, 7028.
(10) (a) Ishii, N.; Ishida, T.; Nogami, T. *Inorg. Chem.* **2006**, *45*, 3837. (b) Ishii, N.; Okamura, Y.; Chiba, S.; Nogami, T.; Ishida, T. *J. Am. Chem. Soc.* **2008**, *130*, 24.

10.1021/cm703530n CCC: $40.75
Published on Web 04/17/2008

we have synthesized a dysprosium analogue $[Dy_2Cu_2]_n$, and preliminary X-ray diffraction studies on $[Dy_2Cu_2]_n$ and $[Gd_2Cu_2]_n$ revealed their similar cell constants.[13] The pulsed-field magnetization curve measurements showed magnetization steps due to the quantum tunneling of magnetization (QTM) for $[Dy_2Cu_2]_n$ as well as monomeric $[Dy_2Cu_2]$ prototypes.[13] The exchange coupling constants are still uncertain because there are two types of exchange paths in the quasi-diamond-arrayed motif. To breakthrough this difficulty, we applied a high-frequency EPR (HF-EPR) technique.

We report here the synthesis and detailed structural characterization of $[Dy_2Cu_2]_n$. The results of ac/dc magnetic susceptibility, magnetization, and HF-EPR are presented. The analysis of EPR is given by using our effective Ising model, and the exchange couplings between Dy and Cu ions are precisely evaluated. This work will certify the generality of the basic idea on the exchange-coupled QTM mechanism originally proposed for [DyCuDy][6] and $[Dy_4Cu]$.[7]

A number of 4f-based SMMs and 4f−3d heterometallic SMMs are known to date,[14–27] but the magnitude of intramolecular exchange coupling has rarely been determined to our knowledge.[6,7] The advantages of HF-EPR are the extremely high resolution,[28] the ability to identify quantum numbers of energy levels by the EPR selection rule, and the observation of the energy level splitting in the excited states. The last point complements the magnetization measurements which clarify the alternation of the ground state (level crossing) from magnetization steps. The EPR technique and related analysis scheme have been established in the determination of spin Hamiltonian parameters of 3d-based SMMs and SCMs, such as the zero-field splitting anisotropy on $[Mn_{12}]$.[29] On the other hand, EPR techniques have been hardly applied to 4f−3d heterometallic systems so far, mostly because of the difficulty of experiments and the lack in analysis methodology. The present case is the first application of EPR for the evaluation of exchange coupling in this type of compound, and therefore this work will provide a standard method for the systematic study on exchange couplings in 4f−3d heterometallic compounds.

Experimental Section

Preparation. Complex $[Dy_2Cu_2]_n$ ($[\{Dy(hfac)_2(CH_3OH)\}_2\{Cu(dmg)(Hdmg)\}_2]_n$) was synthesized by the complexation of $[Dy(hfac)_3(H_2O)_2]$[30] and partially deprotonated $[Cu(Hdmg)_2]$[31] in methanol/acetone (hfac stands for 1,1,1,5,5,5-hexafluoropentane-2,4-dionate). $[Cu(Hdmg)_2]$ (15 mg, 0.050 mmol) was dissolved in 1 mL of MeOH containing 0.1 mmol of KOH. An acetone solution (2 mL) of $[Dy(hfac)_3(H_2O)_2]$ (107 mg, 0.130 mmol) was slowly added to the above solution. The resultant dark brown solution was allowed to stand at room temperature for a day, to give dark brown prismatic crystals that were collected on a filter, washed with a small amount of MeOH, and dried in air. The yield was 27 mg (0.015 mmol; 60% on the repeating unit basis). The elemental analysis (C, H, N) of the complex on a Fisons EA-1108 by a usual combustion method supported the chemical composition. Anal. Calcd C, 25.32; H, 2.12; N, 6.22% for $C_{19}H_{19}CuDyF_{12}N_4O_9$. Found: C, 25.05; H, 2.10; N, 6.10%. IR (KBr disk) 3431, 1655, 1552, 1531, 1491, 1257, 1205, 1147, 1103, 1078, 964, 800, 741, 661, 586, and 486 cm^{-1}.

X-ray Crystallographic Study. Single-crystal X-ray diffraction data of $[Dy_2Cu_2]_n$ were collected on a Rigaku R-Axis RAPID IP diffractometer at 118(1) K using graphite-monochromated Mo Kα radiation ($\lambda = 0.71069$ Å) and the oscillation scans technique in a range of $0 < 2\theta < 56.6°$. The structure was solved by a direct method using the program SIR92[32] and refined by full-matrix least-squares method on F^2 using the program CrystalStructure.[33] Non-hydrogen atoms were refined anisotropically, while hydrogen atoms

(11) (a) Prado, E.; Ruiz-García, R.; Lloret, F.; Faus, J.; Julve, M.; Journaux, Y.; Delgado, F.; Ruiz-Pérez, C. *Adv. Mater.* **2004**, *16*, 1597. (b) Pardo, E.; Ruiz-García, R.; Lloret, F.; Faus, J.; Julve, M.; Journaux, Y.; Novak, M. A.; Delgado, F. S.; Ruiz-Pérez, C. *Chem. Eur. J.* **2007**, *13*, 2054. (c) Toma, L. M.; Lescouëzec, R.; Pasán, J.; Ruiz-Pérez, C.; Vaissermann, J.; Cano, J.; Carrasco, R.; Wernsdorfer, W.; Lloret, F.; Julve, M. *J. Am. Chem. Soc.* **2006**, *128*, 4842.
(12) Ueki, S.; Kobayashi, Y.; Ishida, T.; Nogami, T. *Chem. Commun.* **2005**, 5223.
(13) Ueki, S.; Okazawa, A.; Ishida, T.; Nogami, T.; Nojiri, H. *Polyhedron* **2007**, *26*, 1970.
(14) (a) Osa, S.; Kido, T.; Matsumoto, N.; Re, N.; Pochaba, A.; Mrozinski, J. *J. Am. Chem. Soc.* **2004**, *126*, 420. (b) Hamamatsu, T.; Yabe, K.; Towatari, M.; Osa, S.; Matsumoto, N.; Re, N.; Pochaba, A.; Mrozinski, J.; Gallani, J.-L.; Barla, A.; Imperia, P.; Paulsen, C.; Kappler, J.-P. *Inorg. Chem.* **2007**, *46*, 4458.
(15) (a) Zaleski, C. M.; Depperman, E. C.; Kampf, J. W.; Kirk, M. L.; Pecoraro, V. L. *Angew. Chem., Int. Ed.* **2004**, *43*, 3912. (b) Zaleski, C. M.; Kampf, J. W.; Mallah, T.; Kirk, M. L.; Pecoraro, V. L. *Inorg. Chem.* **2007**, *46*, 1954. (c) Zaleski, C. M.; Depperman, E. C.; Kampf, J. W.; Kirk, M. L.; Pecoraro, V. L. *Inorg. Chem.* **2006**, *45*, 10022.
(16) (a) Mishra, A.; Wernsdorfer, W.; Abboud, K. A.; Christou, G. *J. Am. Chem. Soc.* **2004**, *126*, 15648. (b) Mishra, A.; Wernsdorfer, W.; Parsons, S.; Christou, G.; Brechin, E. K. *Chem. Commun.* **2005**, 2086. (c) Murugesu, M.; Mishra, A.; Wernsdorfer, W.; Abboud, K. A.; Christou, G. *Polyhedron* **2006**, *25*, 613. (d) Mishra, A.; Tasiopoulos, A. J.; Wernsdorfer, W.; Abboud, K. A.; Christou, G. *Inorg. Chem.* **2007**, *46*, 3105.
(17) (a) Ishikawa, N.; Sugita, M.; Ishikawa, T.; Koshihara, S.-Y.; Kaizu, Y. *J. Am. Chem. Soc.* **2003**, *125*, 8694. (b) Ishikawa, N.; Sugita, M.; Wernsdorfer, W. *J. Am. Chem. Soc.* **2005**, *127*, 3650. (c) Ishikawa, N.; Sugita, M.; Tanaka, N.; Ishikawa, T.; Koshihara, S.-Y.; Kaizu, Y. *Inorg. Chem.* **2004**, *43*, 5498.
(18) (a) Costes, J. P.; Dahan, F.; Wernsdorfer, W. *Inorg. Chem.* **2006**, *45*, 5. (b) Costes, J. P.; Auchel, M.; Dahan, F.; Peyrou, V.; Shova, S.; Wernsdorfer, W. *Inorg. Chem.* **2006**, *45*, 1924.
(19) Tang, J.; Hewitt, I.; Madhu, N. T.; Chastanet, G.; Wernsdorfer, W.; Ansen, C. E.; Benelli, C.; Sessoli, R.; Powell, A. K. *Angew. Chem., Int. Ed.* **2006**, *45*, 1729.
(20) (a) Bogani, L.; Sangregorio, C.; Sessoli, R.; Gatteschi, D. *Angew. Chem., Int. Ed.* **2005**, *44*, 5817. (b) Bernot, K.; Bogani, L.; Caneschi, A.; Gatteschi, D.; Sessoli, R. *J. Am. Chem. Soc.* **2006**, *128*, 7947.
(21) (a) Aronica, C.; Pilet, G.; Chastanet, G.; Wernsdorfer, W.; Jacquot, J.-F.; Luneau, D. *Angew. Chem., Int. Ed.* **2006**, *45*, 4659. (b) Aronica, C.; Chastanet, G.; Pilet, G.; Le Guennic, B.; Robert, V.; Wernsdorfer, W.; Luneau, D. *Inorg. Chem.* **2007**, *46*, 6108.
(22) He, F.; Tong, M.-L.; Chen, X.-M. *Inorg. Chem.* **2005**, *44*, 8285.
(23) (a) Mori, F.; Ishida, T.; Nogami, T. *Polyhedron* **2005**, *24*, 2588. (b) Ueki, S.; Sahlan, M.; Ishida, T.; Nogami, T. *Synth. Met.* **2005**, *154*, 217.
(24) Ueki, S.; Ishida, T.; Nogami, T.; Tamura, M. *Mol. Cryst. Liq. Cryst.* **2006**, *455*, 129.
(25) Ferbinteanu, M.; Kajiwara, T.; Choi, K.-Y.; Nojiri, H.; Nakamoto, A.; Kojima, N.; Cimpoesu, F.; Fujimura, Y.; Takaishi, S.; Yamashita, M. *J. Am. Chem. Soc.* **2006**, *128*, 9008.
(26) Pointillart, F.; Bernot, K.; Sessoli, R.; Gatteschi, D. *Chem. Eur. J.* **2007**, *13*, 1602.
(27) Chandrasekhar, V.; Pandian, B. M.; Azhakar, R.; Vittal, J. J.; Clérac, R. *Inorg. Chem.* **2007**, *46*, 5140.
(28) Eaton, G. R.; Eaton, S. S. *Appl. Magn. Reson.* **1999**, *16*, 161.
(29) Barra, A. L.; Caneschi, A.; Cornia, A.; De Biani, F. F.; Gatteschi, D.; Sangregorio, C.; Sessoli, R.; Sorace, L. *J. Am. Chem. Soc.* **1999**, *121*, 5302.
(30) Richardson, M. F.; Wagner, W. F.; Sands, D. E. *J. Inorg. Nucl. Chem.* **1968**, *30*, 1275.
(31) Villa, J. F.; Hatfield, W. E. *J. Chem. Phys.* **1971**, *55*, 4758.
(32) Altomare, A.; Cascarano, G.; Giacovazzo, C.; Guagliardi, A.; Burla, M.; Polidori, G.; Camalli, M. *J. Appl. Crystallogr.* **1994**, *27*, 435.
(33) *CrystalStructure, Crystal Structure Analysis Package*, version 3.8; Rigaku and Rigaku/MSC: The Woodlands, TX, 2000−2006.

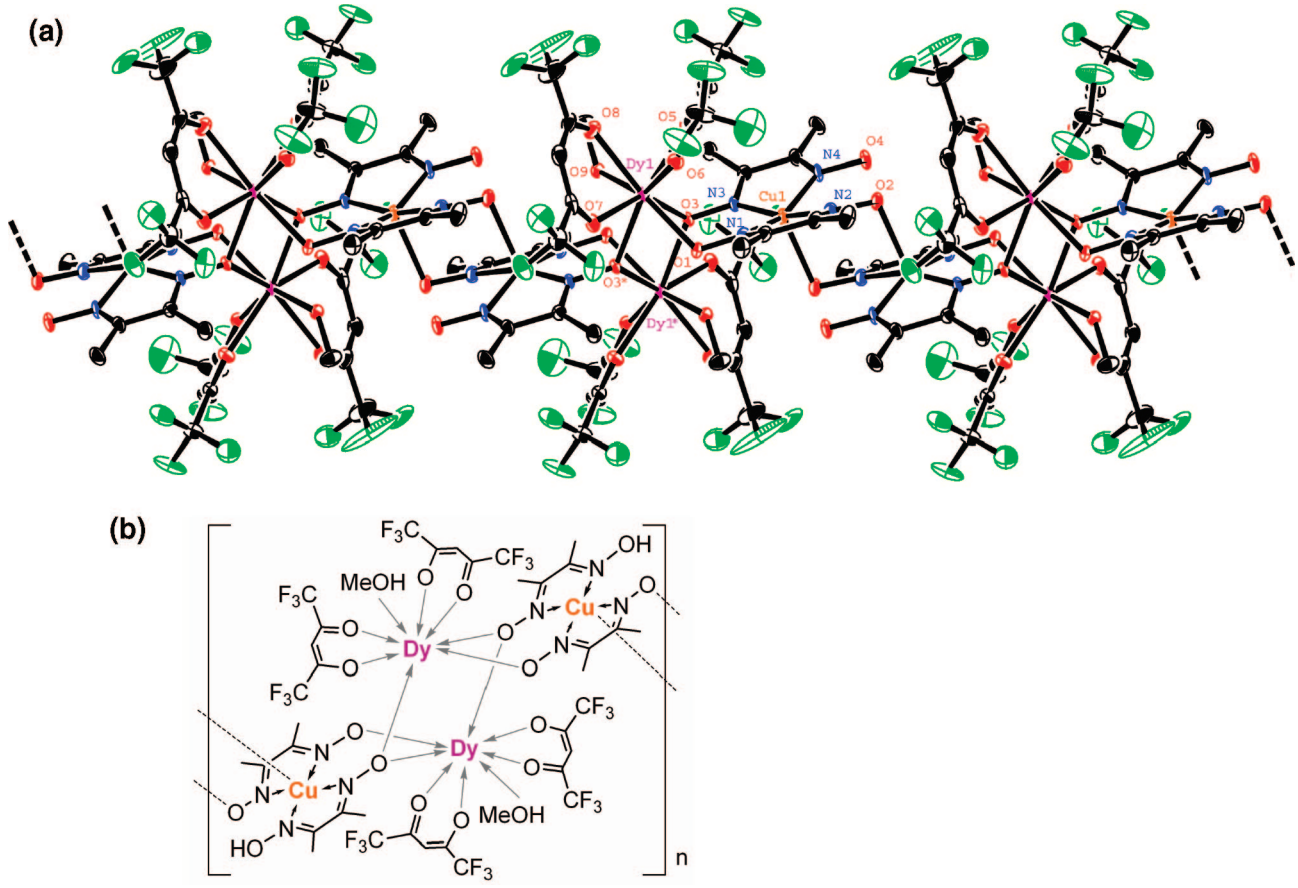

Figure 1. (a) Crystal structure of $[\{Dy(hfac)_2(CH_3OH)\}_2\{Cu(dmg)(Hdmg)\}_2]_n$ ($[Dy_2Cu_2]_n$) with the thermal ellipsoids at the 50% probability level. Three repeating units are shown. Hydrogen atoms are omitted for clarity. Selected atoms are labeled. The symmetry operation code of * is $2 - x$, $1 - y$, $-z$. (b) Structural formula for $[Dy_2Cu_2]_n$.

were located at calculated positions and their parameters were refined as "riding". Selected crystallographic data are as follows. $C_{19}H_{19}CuDyF_{12}N_4O_9$, triclinic, $P\bar{1}$, $a = 10.5791(9)$, $b = 11.0987(13)$, $c = 14.1662(12)$ Å, $\alpha = 71.530(4)$, $\beta = 75.669(3)$, $\gamma = 84.702(5)°$, $Z = 2$, $d_{calcd} = 1.959$ g cm^{-3}, μ(Mo Kα) = 3.249 mm^{-1}, $T = 118$ K, $R_{int} = 0.081$, $R(F)$ ($I > 2\sigma(I)$) = 0.0615, and $R_w(F^2)$ (all data) = 0.0889 for 7318 unique reflections.

Physical Measurements. DC magnetic susceptibilities of $[Dy_2Cu_2]_n$ in a range of 1.8−300 K were measured on a Quantum Design SQUID magnetometer (MPMS-7). Polycrystalline samples were suspended in a small amount of mineral oil "Nujol" (Aldrich). Typical sample masses were 20−50 mg. The magnetization curves were recorded from −70 to +70 kOe. Magnetizations and susceptibilities on randomly oriented polycrystalline specimens were collected after the sample suspension was solidified on cooling without any applied magnetic field. Field-oriented data were obtained after the sample suspension was solidified in the applied field of 7 T. As for single-crystal magnetization measurements, a black prismatic crystal (0.33 × 0.60 × 0.18 mm^3) was fixed with a small amount of vacuum silicon grease. The ac measurements were obtained on a Quantum Design PPMS ac/dc magnetometer on polycrystalline samples fixed in mineral oil. The ac frequency varied from 50 to 10 000 Hz with an amplitude of 5 Oe.

Low-temperature magnetization was measured by a conventional inductive probe in pulsed-magnetic fields, and the temperature reached was as low as 0.5 K using a ^{3}He cryostat.[34] Polycrystalline specimens (typically 15 mg) were mounted in a capillary made of polyimide Kapton (duPont). The sample was not fixed within the sample tube, and then it aligned along the magnetic field direction. After we applied the magnetic field several times, the orientation effect was saturated, and the magnetization curves obtained in further shots were found to be identical.

HF-EPR spectra for polycrystalline samples were obtained on the same pulsed-field generator.[35] The sample was packed in a case made of polyethylene. The radiation was produced by Gunn oscillators, backward traveling wave oscillators, and an optically pumped far-infrared laser.

Results

Crystal Structure. The cell parameters of $[Dy_2Cu_2]_n$ have been reported preliminarily,[13] and we have now determined the precise atomic positions from the single-crystal X-ray diffraction study. The molecular and crystal structures of $[Dy_2Cu_2]_n$ (Figure 1) are practically identical with the known $[Gd_2Cu_2]_n$,[12] except for the absence of any crystal solvent molecules. The complex crystallizes in a $P\bar{1}$ space group. A partially deprotonated $[Cu(dmg)(Hdmg)]^-$ unit is coordinated to two Dy^{3+} ions through the oximate oxygen atoms, and thus the oximate bridge (Dy−O−N−Cu) is found in every nearest Dy···Cu geometry. A discrete polymeric chain, constructed with a Cu···Cu linkage, runs along the crystallographic b axis.

(34) Nojiri, H.; Choi, K.-Y.; Kitamura, N. *J. Magn. Magn. Mater.* **2007**, *310*, 1468.

(35) Nojiri, H.; Ajiro, Y.; Asano, T.; Boucher, J.-P. *New J. Phys.* **2006**, *8*, 218.

The Dy^{3+} ion is eight-coordinated by oxygen atoms from one MeOH molecule, two bridging oxime groups, and two hfac ligands, forming an approximate D_{4d} square-antiprism (SAPR) coordination sphere with an axial compression. The two SAPR polyhedra are fused with two oxygen atoms (O3 and O3*) shared. The Dy1−O1, Dy1−O3, and Dy1*−O3 distances are 2.331(6), 2.427(5), and 2.356(5) Å, respectively. Other Dy−O distances range from 2.313(6) to 2.409(7) Å.

The $[Dy_2Cu_2]$ unit is centrosymmetric, and another inversion center resides at the middle of the two Cu ions between neighboring units. Dy1 and Cu1 are doubly bridged with oximate groups (O1−N1 and O3−N3), while Dy1* and Cu1 are singly bridged with an oximate group (O3−N3). The Dy1···Dy1*, Dy1···Cu1, and Dy1*···Cu1 separations are 3.9945(5), 4.0247(9), and 4.5995(11) Å, respectively. The torsion angles of Dy−O−N−Cu are considerably large (−62.3(5), 56.5(5), and −93.3(6)° for Dy1−O1−N1−Cu1, Dy1−O3−N3−Cu1, and Dy1*−O3−N3−Cu1, respectively). The nonplanar Dy−O−N−Cu structure is related with the magnetic coupling operative here.[7,12,36]

The Cu^{2+} ion has a square-pyramidal geometry. The [Cu(dmg)(Hdmg)] moiety forms a sandwich dimer correlated with an inversion symmetry. The basal plane consists of four nitrogen atoms from dmg or Hdmg ligands with the Cu−N bond lengths of 1.969(7)−2.005(8) Å. A neighboring oximate oxygen atom is located at the axial position with a longer distance (2.248(5) Å). The magnetic orbital $3d_{x^2-y^2}$ is located on the basal plane, and accordingly the spin-polarized lone-pair of the oxygen atom of a neighboring molecule is located in an orthogonal manner. This structure favors ferromagnetic coupling.[31] The Cu1···Cu1* separation is 3.8978(14) Å.

To describe the following magnetic properties, we define a repeating unit as a quasi-diamond macrocycle [$CuDy_2Cu$] as shown in the bottom of Figure 1. Intermacrocycle coupling is thus assigned to an interaction between two neighboring Cu ions.

Magnetic Properties. Preliminary dc and ac magnetic susceptibility measurements on a randomly oriented polycrystalline specimen of $[Dy_2Cu_2]_n$ have been reported previously.[13] At room temperature, the $\chi_{mol}T$ value of 32.11 cm^3 K mol^{-1} is close to the calculated value 29.11 cm^3 K mol^{-1} expected for two Cu^{2+} (0.375 cm^3 K mol^{-1} per a Cu^{2+}; $S = 1/2$ and $g = 2.0$) plus two Dy^{3+} ions (14.18 cm^3 K mol^{-1} per a Dy^{3+}; $S_{Dy} = 5/2$, $L_{Dy} = 5$, $J_{Dy} = 15/2$, and $g_J = 4/3$). We have now investigated the magnetic properties of a field-oriented polycrystalline sample of $[Dy_2Cu_2]_n$ (Figure 2a). On cooling, the $\chi_{mol}T$ value once decreased down to 6.5 K, reached a minimum value of 47.6 cm^3 K mol^{-1}, and then turned to increase. The $\chi_{mol}T$ value was 57.5 cm^3 K mol^{-1} at 1.8 K. The upsurge in a low temperature region is similar to that of a randomly oriented specimen,[13] but the present $\chi_{mol}T$ value is almost twice as large as the randomly oriented data. The magnitude of $\chi_{mol}T$ indicates that a ground state of the Dy ions is given by the maximal value of $|J^z| = 15/2$, being well separated from the first excited-state in the $2J + 1$ multiplet series.

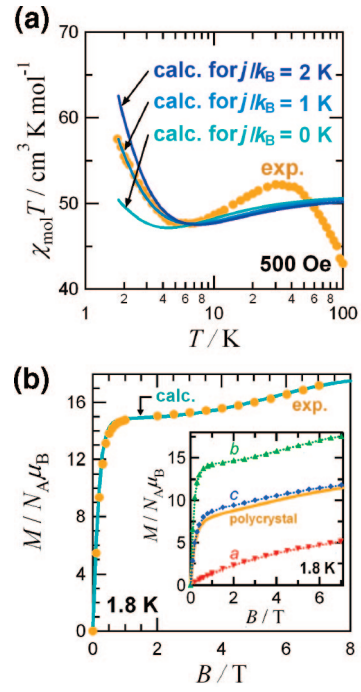

Figure 2. (a) Temperature dependence of $\chi_{mol}T$ for a field-oriented polycrystalline sample of $[Dy_2Cu_2]_n$ at 500 Oe (orange filled circles). Blue solid lines represent simulation curves for a dimmer model $[CuDy_2Cu]_2$ with $J_A/k_B = -0.895$ K, $J_B/k_B = -0.061$ K, and $j/k_B = 0$, +1.0, and +2.0 K. (b) Magnetization curves of a field-oriented polycrystalline sample of $[Dy_2Cu_2]_n$ measured at 1.8 K (orange filled circles) and calculation on the model $[CuDy_2Cu]$ (light blue solid lines). Inset: Magnetization curves of a randomly oriented polycrystalline sample (orange solid line) and a single crystal specimen of $[Dy_2Cu_2]_n$ measured at 1.8 K. The marks *a*, *b*, and *c* indicate the magnetization curves with the applied field parallel to the *a*, *b*, and *c* axes, respectively. Lines are shown for a guide to the eye.

The magnetization curves of a randomly oriented polycrystalline specimen of $[Dy_2Cu_2]_n$ were recorded at 1.8 K (the inset of Figure 2b). No hysteresis was observed with usual field-scan rates on a SQUID magnetometer. To clarify the magnetic anisotropy, we measured magnetization curves on a single crystal. The measurements show that the magnetic easy axis is almost parallel to the crystallographic *b* direction. The magnetization along the *b* axis was almost saturated at 7 T, and this value is smaller than a theoretical saturated one from two Dy^{3+} and Cu^{2+}, suggesting that the Dy^{3+} moment lies in a direction between the *b* and the *c* axes (the former is arranged closer). The magnetization curve showed a step in the measurements along the *b* axis, which can be assigned to the reorientation of the two Cu^{2+} spins. The energy level cross between the ferrimagnetic $[Dy(\uparrow)_2Cu(\downarrow)_2]_n$ and the ferromagnetic $[Dy(\uparrow)_2Cu(\uparrow)_2]_n$ states occurs here with the aid of the Zeeman energy. The curvature averaged over the *a*, *b*, and *c* axis data was practically identical to that of the polycrystalline data. Furthermore, the magnetization curve on a field-oriented specimen (Figure 2b) was also quite similar to that of the *b* axis data on a single-crystal specimen (the inset). The saturation value was as large as 17.7 μ_B, which is about 80% of the full saturation of 22 μ_B, owing to incomplete field-orientation. When the saturation value is calibrated as 22 μ_B, we found that the jump approximately corresponds to 4 μ_B. The reversal of one Cu spin gives a 2 μ_B jump, and thus the 4 μ_B step is caused by the simultaneous flip of two Cu ions per a repeating unit.

(36) Kobayashi, Y.; Ueki, S.; Ishida, T.; Nogami, T. *Chem. Phys. Lett.* **2003**, *378*, 337.

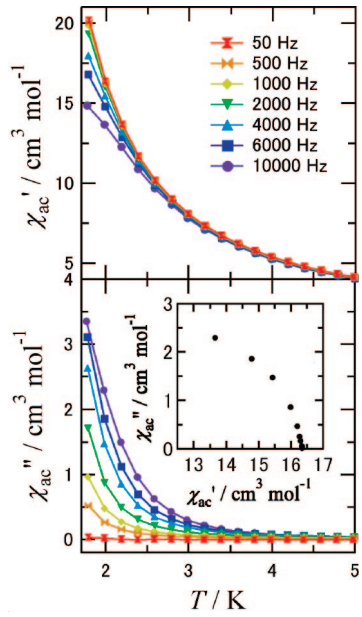

Figure 3. AC magnetic susceptibilities (χ_{ac}' and χ_{ac}'' for in-phase and out-of-phase parts, respectively) for a randomly oriented polycrystalline sample of $[Dy_2Cu_2]_n$. The amplitude of the applied ac magnetic field was 5 Oe. Lines are shown for a guide to the eye. Inset shows the Cole−Cole diagram at 1.8 K.

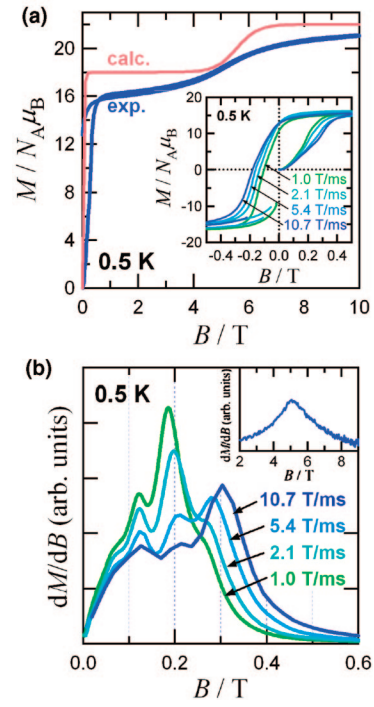

Figure 4. (a) Pulsed-field magnetization curve of $[Dy_2Cu_2]_n$ measured at 0.5 K (blue solid line). A red solid line represents a simulation curve for the model $[CuDy_2Cu]$ at 0.5 K. Inset shows hysteresis curves in a low-field region. (b) Differential magnetization curves as a function of a field-sweeping rate measured at 0.5 K. Inset shows a differential magnetization curve showing a 4-μ_B jump around 5.5 T.

Ac magnetic susceptibilities, χ_{ac}'' and χ_{ac}'' for the in-phase and out-of-phase components, respectively, are plotted as a function of temperature and frequency (Figure 3).[13] We can observe frequency dependence of the ac susceptibilities. With an increase of frequency, a χ_{ac}' decrease and a concomitant χ_{ac}'' increase were clearly observed. We confirmed that the magnetization relaxation became relatively slow, compared with the time scale of these experiments. However, no χ_{ac}'' peak appeared above 1.8 K in our apparatus, and the activation energy of the magnetization reorientation could not be estimated. A Cole−Cole plot[37] displayed an only partial semicircle (the inset of Figure 3). The activation energy of the magnetization reorientation will be estimated by an appropriate model (see below), instead of the Arrhenius analysis.

The pulsed-field technique gave more detailed information on the magnetization process. Figure 4a shows a distinct magnetization step at 5.5 T measured on a polycrystalline sample of $[Dy_2Cu_2]_n$ at 0.5 K, which is much clearer than that measured at 1.8 K (Figure 2b), owing to the suppression of population on thermally activated states. In a small field region, the dM/dB versus B plot (Figure 4b) clarifies mainly four fine magnetization jumps at 0.06, 0.12, 0.19, and 0.26 T at a field scan rate of 1.0 T/ms. This behavior is related with QTM caused by the level crossing among excited states, which is characteristic of SMMs[1−3] and SCMs.[8] The positions of two former steps (0.06 and 0.12 T) are independent of the sweep rate. As for the latter (0.19 and 0.26 T), the positions shift as a function of the sweep rate, presumably because of a nonadiabatic effect. It is also found that hysteresis curves are slightly asymmetric; in the negative field each step was shifted with respect to the positive one, indicating the presence of a dipolar-coupling bias that affects the field at which QTM takes place. The origin of the magnetization step and the fine structure will be discussed together with the results of EPR experiments.

HF-EPR Spectra. HF-EPR spectra for crystalline samples were collected in a wide frequency range between 34.7 and 525.4 GHz and in the corresponding magnetic field range of 0−25 T. Figure 5a shows typical EPR spectra recorded at 4.2 K. The spectrum of 117.4 GHz exhibited two intense peaks at 1.2 and 9.9 T. The band position of the former was abnormally shifted to a lower field with an increase of frequency. On the other hand, the latter moved to a higher field, obeying the Zeeman effect. At 305 GHz, only the higher-field peak was found. On decreasing frequency, the two peaks seem to merge around 5.5 T at zero frequency.

Figure 5b shows an expansion of a low field part of the spectra. We found additional weak absorptions indicated by red arrows in the lower-field side. The intensities of the two major peaks decreased rapidly with elevating temperature, while that of the minor peak was more gradual above 4.2 K. Moreover, the minor peak disappeared at lower temperatures. Those behaviors indicate that the major peaks can be assigned to excitation from the ground state and the minor peak to that from excited states.

The frequency dependence of the absorption positions is summarized in Figure 5c. The peak positions of the major peaks showed a V-shaped pattern. The minor peak was observed only in a low magnetic field region. From linear fits of the slopes for the major and minor bands, we obtained $g = 1.919(3)$ and 2.07(2), respectively. The turning point of the former was 5.56(3) T at zero frequency. The g-values are very close to 2, implying that the observed EPR is caused

(37) Cole, K. S.; Cole, H. R. *J. Chem. Phys.* **1941**, *9*, 341.

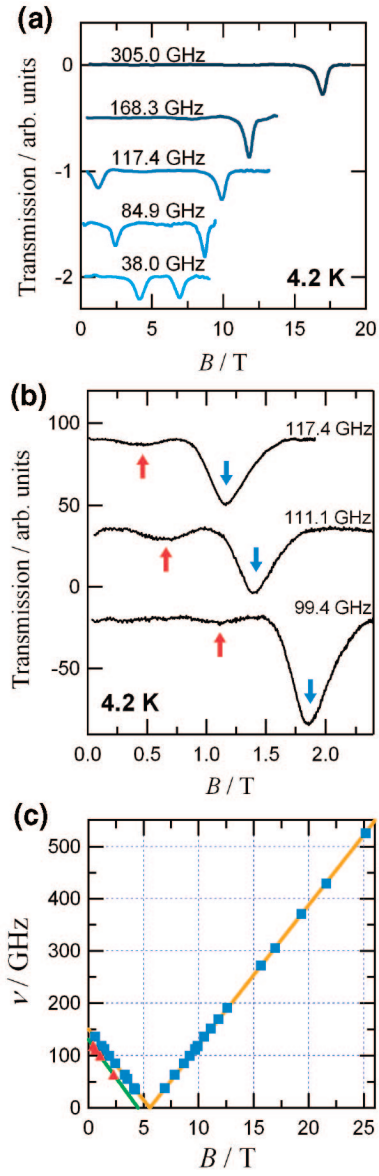

Figure 5. (a) Selected HF-EPR spectra of $[Dy_2Cu_2]_n$ measured at 4.2 K as a function of frequency. (b) Expanded HF-EPR spectra at 4.2 K showing a minor absorption band (denoted with red arrows) together with a major one (blue arrows). (c) Frequency-field diagram of two EPR absorption bands (major, blue filled square; minor, red filled triangle) observed at 4.2 K for $[Dy_2Cu_2]_n$. Solid lines represent the best linear fittings. See the text for the optimized parameters.

by the reversal of a Cu $S = 1/2$ spin consistent with a conventional EPR selection rule of $\Delta m_s = \pm 1$. There is no single-ion type anisotropy in Cu spins, and thus the observed characteristic frequency-field relation shows the presence of internal fields on Cu sites mediated by sizable exchange couplings between Dy and Cu ions.

We can illustrate an energy level diagram together with exchange couplings by analyzing the EPR data. The intercept of the frequency-field diagram usually corresponds to an energy level crossing. In fact, the magnetization step is found in the magnetization curves (Figures 2 and 4a for 1.8 and 0.5 K, respectively) at 5.5 T. The critical fields of two independent methods agree well with each other. The HF-EPR experiments have an advantage in precise determination of the position of the energy level crossing.

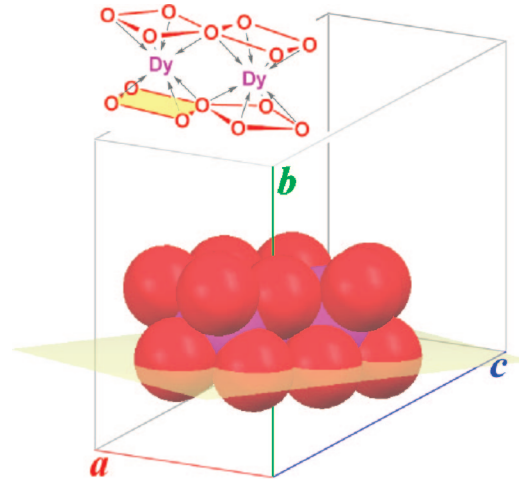

Figure 6. Coordination sphere of the oxygen atoms around the Dy ions and mutual direction with respect to the unit cell in the crystal of $[Dy_2Cu_2]_n$. A yellow plane represents a basal plane of the square antiprism coordination structure defined by O1, O3, O5, and O6.

Discussion

Magnetic Anisotropy. The single-crystal magnetic study on $[Dy_2Cu_2]_n$ (the inset of Figure 2b) revealed that the magnetic easy-axis lies almost along the chain direction (the crystallographic *b* axis). Note that the easy-axis direction of the single ion is unique in the crystal, because there are two Dy^{3+} ions in a unit cell and they are related by an inversion symmetry in the space group $P\bar{1}$. We can define the unique Ising axis for the whole system.

The saturation behavior of the data parallel to the *b* axis supports that the easy axis is correctly found in a real crystal. However, a considerable portion of the magnetization parallel to the *c* axis was also observed, in contrast to the reports on the uniaxial magnetic anisotropy located just in the chain direction for metal−radical SCMs[8] and heterometallic SCMs.[4] The magnetization easy axis was mapped on the X-ray crystal structure for $[Dy_2Cu_2]_n$ to explain the dislocation of the magnetic easy axis of $[Dy_2Cu_2]_n$ from the chain direction. The coordination sphere of the Dy^{3+} ion is an axially compressed SAPR structure. Figure 6 depicts an edge-shared double SAPRs of the Dy_2O_{14} moiety based on the crystallographic analysis. A uniaxial anisotropy has been characterized for the $[Dy(pc)_2]$-type SMM having an N_8 compressed SAPR coordination (pc stands for phthalocyaninate);[17] the magnetic easy axis coincides the SAPR axial direction. Similarly, in the present compound, the uniaxial anisotropy seems to be related to the SAPR axis, which is inclined from the chain direction (i.e., the *b* axis direction) to the *c* direction by approximately 10°. Furthermore, the α angle is 71.530(4)° in the triclinic cell (Figure 6), and consequently almost a half amount of the Dy^{3+} moments would be detected along the *c* axis compared with that of the *b* axis. The experimental results shown in the inset of Figure 2b are fully compatible with this picture. The strong uniaxial anisotropy guarantees that each Dy^{3+} moment can be treated as an Ising spin in the following discussion.

Ferrimagnetic Ground State and Exchange Coupling. We can find a magnetization step in Figure 4a which corresponds to the Cu spin-flip by 4 μ_B, definitely indicating

the ground ferrimagnetic state of $[Dy(\uparrow)_2Cu(\downarrow)_2]$ for a unit. Very similarly, the corresponding monomeric prototypes $[\{Dy(hfac)_2(ROH)\}_2\{Cu(emg)(Hemg)(ROH)\}_2]$ (R = CH_3 and C_2H_5; H_2emg stands for ethylmethylglyoxime) have been established to be ground ferrimagnetic compounds as $[Dy(\uparrow)_2Cu(\downarrow)_2]$.[13] We measured the $\chi_{mol}-T$ data and magnetization curves on a field-oriented specimen of $[Dy_2Cu_2]_n$. The upturn of the $\chi_{mol}T$ value observed below 6.5 K (Figure 2a) is consistent with the fact that the ground state is ferrimagnetic.

It is not clear whether the Dy−O−Dy bridge transmits a ferromagnetic coupling, but it is reasonably acceptable that two Dy spins with an intervening Cu spin are ferrimagnetically correlated as Dy(↑)−Cu(↓)−Dy(↑). Although there have been several examples showing ferromagnetic coupling of heavier lanthanide ions (including Gd and Dy) with Cu ions, the antiferromagnetic coupling between Dy and Cu ions across the oximate O−N bridge have been discussed[6,7,12] based on the twisted geometry[38] defined by the Dy−O−N−Cu torsion and comparison with the Gd and heavier lanthanide analogues.[39] The nonplanar Dy−O−N−Cu structures in $[Dy_2Cu_2]_n$ favor antiferromagnetic coupling.

On the other hand, the intermacrocycle Cu···Cu coupling is ferromagnetic according to a superexchange mechanism. Hatfield et al. also reported the ferromagnetic coupling in the synthetic precursor $[Cu(dmgH)_2]_2$.[31] Several dinuclear copper(II) compounds having out-of-plane-bridged structures are known to show ferromagnetic interaction between the two Cu ions.[40] In the Gd analogue, it has been already proved that the $\{Cu(dmg)_2\}_2$ dimerization gives rise to ferromagnetic coupling therein.[12] Experimentally, the ferromagnetic coupling was confirmed in the initial steep raise of the magnetization as well as the hysteresis loop in the low-temperature magnetization curves. If an antiferromagnetic coupling was present between Cu ions, a gradual increase of magnetization would be recorded.

Each chain is sufficiently isolated in the crystal packing owing to the bulky substituents such as CF_3. The exchange coupling between 4f metal ions are much smaller than the 4f−3d and 3d−3d interactions.[41] We propose models of the exchange couplings in $[Dy_2Cu_2]_n$ as shown in Figure 7. Interaction of a diagonal Cu···Cu is disregarded from viewing of the long distance. In a tetranuclear model, two exchange couplings between Dy and Cu ions are considered (J_A and J_B), which are crystallographically independent. This magnetic model may be better described as a rectangle rather than a diamond. When the diamond-arrayed units form a chain, an additional coupling j across the Cu···Cu linkage should be taken into account. As long as the j is small and ferromagnetic, it gives a shift of the energy of the ferrimagnetic ground-state as a whole, but an energy diagram around low-lying states is only slightly modified when infinite

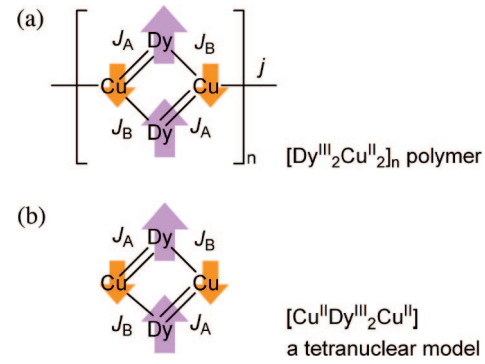

Figure 7. (a) Exchange coupling scheme for $[Dy_2Cu_2]_n$. (b) A tetranuclear model $[CuDy_2Cu]$.

systems are constructed.[42] We can easily corroborate it by calculating the energy levels for a finite chain with periodic boundary conditions including two or three units (see below). The spin structure overlaid in Figure 7a is qualitatively plausible.

Effective Ising Model. A Dy moment with total J (= L + S) splits into $2J + 1$ multiplets owing to the strong anisotropy. If the temperature is sufficiently below the energy separation between the ground state and the excited states, the J of each Dy ion can take only the ground-state value. It means that the full Hamiltonian of the system can be reduced to an effective Hamiltonian, in which the J value is fixed to that of the ground state. When the symmetry of the ground state is reasonably high, the ground state may be one of the doublets such as $|J^z| = 15/2$; in other words, the Dy moment can be treated as an Ising spin. Note that the present experiments were done at low temperatures, and thus this simplification is realistic even if there is some distortion of symmetry. Such Ising models were recently proposed by us in the analysis of 4f-3d heterometallic SMMs, and the exchange couplings have been successfully evaluated.[6,7] Those models involved only one exchange coupling as an adjustable parameter, but we have to extend the model to include two different exchange couplings in the present work. We propose the following Hamiltonian for the tetranuclear $[CuDy_2Cu]$ unit.

$$\hat{H} = -J_A(\hat{J}_2^z \bullet \hat{S}_1 + \hat{J}_3^z \bullet \hat{S}_4) - J_B(\hat{J}_3^z \bullet \hat{S}_1 + \hat{J}_2^z \bullet \hat{S}_4) + \mu_B H^z(g_1 S_1 + g_2 J_2^z + g_3 J_3^z + g_4 S_4) \quad (1)$$

Symbols J_2 and J_3 represent the total moments of Dy ions, while S_1 and S_4 represent the spins of Cu ions. The first and second terms stand for the Ising type exchange interactions between Dy and Cu ions, where the coupling parameters are defined as $-J_A$ and $-J_B$, and the third term represents the Zeeman interaction. As mentioned previously, it suffices to consider a coupling between a ground doublet state of the Dy ions having $|J^z| = 15/2$. Here the exchange coupling term is an originally isotropic Heisenberg type formula; however, the resultant energy level in the Hamiltonian is that of the Ising model. The dipolar interactions are disregarded.

(38) (a) Costes, J.-P.; Dahan, F.; Dupuis, A.; Laurent, J.-P. *Inorg. Chem.* **2000**, *39*, 169. (b) Costes, J.-P.; Dahan, F.; Dupuis, A. *Inorg. Chem.* **2000**, *39*, 5994.
(39) Kahn, M. L.; Mathoniere, C.; Kahn, O. *Inorg. Chem.* **1999**, *38*, 3692.
(40) Cervera, B.; Ruiz, R.; Lloret, F.; Julve, M.; Cano, J.; Faus, J.; Bois, C.; Mrozinski, J. *J. Chem. Soc., Dalton Trans.* **1997**, 395.
(41) Panagiotopoulos, A.; Zafiropoulos, T. F.; Perlepes, S. P.; Bakalbassis, E.; Masson-Ramade, I.; Kahn, O.; Terzis, A.; Raptopoulou, C. P. *Inorg. Chem.* **1995**, *34*, 4918.
(42) Oshima, Y.; Nojiri, H.; Asakura, K.; Sakai, T.; Yamashita, M.; Miyasaka, H. *Phys. Rev. B* **2006**, *73*, 214435.

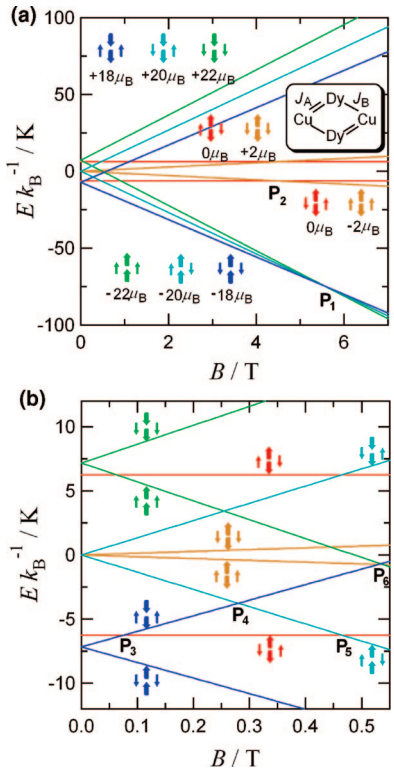

Figure 8. (a) Energy levels of a tetranuclear model $[CuDy_2Cu]$ in a ground-state manifold calculated by the spin Hamiltonian (see the text). (b) Magnification of the plot in a low field region. Spin structures are drawn with arrows. One of the degenerate states is shown; for example, the $M^z = -2\ \mu_B$ state is 2-fold degenerate.

One may point out the possibility of an admixture of J^z levels or the ground $|J^z|$ value other than 15/2.[43] There are some supports for the ground state of $|J^z| = 15/2$. We found the normalized saturation magnetization to be 22 μ_B when the normalization factor was determined from the jump of 4 μ_B for the reversal of two Cu^{2+} spins. The second point is the g-value close to 2 and the straight frequency-field relation found in the EPR experiments. If the ground-state is different from $|J^z| = 15/2$, the g-value cannot be close to 2. Moreover, admixtures of different $|J^z|$ values would result in the additional zero-field splitting of the doublet. In this case, the energy level should bend around zero field, but such a feature is totally absent in the experiments.

Evaluation of Exchange Parameters. Figure 8a shows the energy levels of the $[CuDy_2Cu]$ model calculated on the basis of eq 1. Here we use the values $J_A/k_B = -0.895$ K, $J_B/k_B = -0.061$ K, $J_2^z = J_3^z = 15/2$, $S_1 = S_4 = 1/2$, $g_2 = g_3 = g_{Dy} = 4/3$, and $g_2 = g_3 = g_{Cu} = 1.919$ or 2.07. Those parameters are chosen to fit the EPR and magnetization data as we discuss below.

The exchange interaction energy of a neighboring Dy−Cu is defined with $-J(J^z \cdot S)$. In the tetranuclear unit, each Dy or Cu moment can point up or down, and consequently the total number of states is $2^4 = 16$. Since the Landé g factors for lanthanide ions do not equal to 2, it is a convenient way to use a quantum number M to be equivalent to $g_J J$, that is, a Dy ion has 10 μ_B. Thus, in zero field, the energy of the ground ferrimagnetic $|M^z| = 18\ \mu_B$ state ([Cu(↓)Dy(↑)Dy(↑)-Cu(↓)]) is lower than that of an $|M^z| = 20\ \mu_B$ state ([Cu-(↑)Dy(↑)Dy(↑)Cu(↓)] for example) by $-2(J_A + J_B)J^z \cdot S$. Similarly, the energy of an excited ferromagnetic $|M^z| = 22$ μ_B state ([Cu(↑)Dy(↑)Dy(↑)Cu(↑)]) is higher than that of an $|M^z| = 20\ \mu_B$ state by the same gap. Spin arrangements are schematically drawn by arrows in Figure 8. Each of those states splits to two states owing to the Zeeman effect. Considering the selection rule of EPR ($\Delta m_s = \pm 1$), we can expect the transitions between the states of $M^z = -18$ and $-20\ \mu_B$ and between those of $M^z = -20$ and $-22\ \mu_B$. Those two transitions show the identical field dependence. Namely, the zero-field offsets of two modes decrease on applying a magnetic field and become zero at the same field. Therefore, the two EPR signals intrinsically overlap at any frequency, and the levels are crossing at the same position (P_1). On further increasing a magnetic field from P_1, the energy of the transition increases linearly, being fully consistent with the V-shaped frequency−field relation for the major peaks.

The experiments revealed the energy level cross among the three states ($M^z = -18$, -20, and $-22\ \mu_B$) at 5.56(3) T and the g_{Cu} value of 1.919(3), leading to the energy gap $-2(J_A + J_B)J^z \cdot S$ of 7.17(4) K. Since three states are separated equally, the determination of the level crossing field tells only the sum of J_A and J_B. We cannot separate J_A and J_B at this stage, even when the results of the magnetic study are combined.

There is another EPR absorption satisfying the selection rule, that is, transitions from $M^z = 0$ to $-2\ \mu_B$ and $M^z = +2$ to 0 μ_B. We can deduce that the minor band is attributed to the absorption of these transitions. As shown in Figure 8, there are three states at zero field. The zero-field energy of the $|M^z| = 2\ \mu_B$ state ([Cu(↑)Dy(↑)Dy(↓)Cu(↑)], for example) is exactly zero for the cancelation of J_A and J_B, and this state undergoes the Zeeman splitting. In case of the singlet states ($M^z = 0\ \mu_B$), the zero-field offsets from the $|M^z| = 2$ μ_B level are given by the difference of two exchange couplings as $-2(J_A - J_B)J^z \cdot S$. Since the three states are equally spaced at zero field, two transitions show the identical field dependence. The zero-field offset is calculated to be 6.25(8) K from 4.50(6) T with $g_{Cu} = 2.07(2)$. From a combination of the equations, $-(15/2)(J_A + J_B)/k_B = 7.17(4)$ K and $-(15/2)(J_A - J_B)/k_B = 6.25(8)$ K, we successfully obtain $J_A/k_B = -0.895(8)$ K and $J_B/k_B = -0.061(8)$ K.

We can assign the minor band to absorptions between the excited states. The intensity ratio of minor/major EPR signals is quantitatively consistent with the estimation by using Boltzman's function. Assuming that the signal intensity is proportional to the Boltzman distribution at each state, we calculated the ratio of the minor/major bands, giving 8.9×10^{-2}, 3.5×10^{-2}, and 4.2×10^{-3} at 4.2 K with the frequencies of 117.4, 111.1, and 99.4 GHz, respectively. The observed ratios were 5.5×10^{-2}, 2.7×10^{-2}, and 8.6×10^{-3} (Figure 5b), respectively, in agreement with the calculation within an appreciable error in reading the intensity. Furthermore, with an increase of the field we could not follow the minor band because of the negligible intensity. It is consistent with the Zeeman effect leading to the $M^z =$

(43) Sugita, M.; Ishikawa, N.; Ishikawa, T.; Koshihara, S.-Y.; Kaizu, Y. *Inorg. Chem.* **2006**, *45*, 1299.

−2, 0, and 2 μ_B states being much more stabilized than the $M^z = -18$, −20, and −22 μ_B ones in higher fields (Figure 8a).

These g values are close to 2, supporting the assignment of this absorption to the flip of a Cu^{2+} spin. In detailed discussion, the g value of the minor band (2.07(2)) is somewhat larger than that of the major band (1.919(3)), being consistent with the fact that the former is purely originated from the Cu^{2+} g value when the Dy^{3+} spins are completely canceled in the corresponding states. The principal axis direction of the Cu^{2+} ion differs from the Dy^{3+} one. Namely, the Dy^{3+} easy axis is approximately parallel to the Cu^{2+} basal plane (Figure 1). When the Cu^{2+} spin is exchange-coupled with the Ising Dy^{3+} spins in the states of $M^z = -18$, −20, and −22 μ_B, the g value should be observed as $g_\perp$, which is smaller than $g_{||}$ for typical Cu^{2+} coordination compounds having a magnetic $3d_{x^2-y^2}$ orbital.[44] The slightly smaller g value for the major band supports the presence of exchange coupling with adjacent Dy^{3+} ions.

The exchange parameters in the present compound are comparable to those of the previous compounds; −0.64 K for $[Dy_4Cu]$[7] and −0.115 K for [DyCuDy].[6] The former has double oximate bridges, while the latter a single oximate bridge. Only from the analysis on the present compound never can we tell a priori which value, J_A or J_B, would be assigned to each crystallographically independent Dy−O−N−Cu relation. However, the negatively larger one (J_A) is likely ascribable to the coupling across double oximate bridges, because of the same order of the J values, and the smaller one (J_B) to the coupling across a single bridge.

We make a brief comment on blocking. As Figure 8b shows, the first excited state is located at only 0.92 K higher than the ground-state level at zero field. This value can be regarded as a lowest activation energy for the magnetization reorientation. A possible blocking seems to occur much below 1.8 K (Figure 3). The activation energy could not be determined by the Arrhenius analysis from the χ_{ac} data, simply because it is as small as 0.92 K.

Estimation of Intermacrocycle Interaction. To clarify the magnitude of the intermacrocycle interaction (j), we proposed here a dimeric octanuclear model $[CuDy_2Cu]_2$, introducing periodic boundary conditions. Figure 9 shows the energy diagram for $[CuDy_2Cu]_2$ with $J_A/k_B = -0.895$ K, $J_B/k_B = -0.061$ K, and $j/k_B = +1.0$ K. Though there are many levels due to eight doublets, we concentrate on a few low-lying lines, because the observed magnetization is dominantly contributed to by low-lying states. The energy structure near the ground state was hardly changed, and the level-crossing field was not shifted (5.56 T). Calculated magnetization curves of $[CuDy_2Cu]$ and $[CuDy_2Cu]_2$ at 0.5 or 1.8 K were practically identical to each other and reproduced well the experimental curve of $[Dy_2Cu_2]_n$ (Figure 4a). It should be noted that, since the calculations on the tetra- and octanuclear models exhibited practically no size effect in the magnetization, extrapolation to an infinite polymer would also give a similar result.

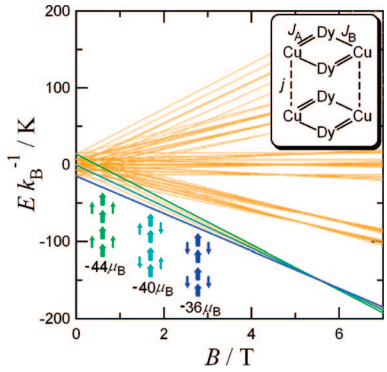

Figure 9. Calculated energy levels of a dimeric octanuclear model $[CuDy_2Cu]_2$. Selected spin structures are drawn with arrows.

It was rather difficult to determine the magnitude of j solely from the magnetization and EPR analyses. On the other hand, the $\chi_{mol}T$ versus T plot in a lowest temperature region is very sensitive to j, because the ground ferrimagnetic moment remarkably increases with an increase of j. Actually, a simulation work tells us that the larger j value leads to the sharper upsurge of the $\chi_{mol}T$ value around 2 K, as shown by calculated curves for the octanuclear model with $j/k_B = 0$, +1, and +2 K (Figure 2a). A fit to the experimental $\chi_{mol}T$ value approximately gave $j/k_B = +1.0$ K. The experimental value was somewhat smaller than the calculated curves by a factor of 0.689, because of the incomplete field orientation. A broad minimum typical of ferrimagnetic chains is found around 6 K. The Ising character of the Dy spins cannot be held at higher temperatures, the easy-axis component of the moments is decreased, and accordingly the $\chi_{mol}T$ value in this direction is deviated downward on heating above approximately 50 K.

There are many examples of dinuclear Cu^{2+} complexes involving out-of-plane oximate bridges which showed ferromagnetic coupling, and the magnitude of the coupling depends on the geometry.[40] The present value falls in a typical range of the Cu−Cu coupling,[31,40] indicating that the present simulation is reliable.

Fine Structure in the Magnetization. Finally we will discuss the energy level crossings taking place in a small field region. The magnetization jumps were found in the pulsed-field experiments (Figure 4b). The calculated energy level crossings are shown in Figure 8b. Important crossings are P_3 (0.08 T), P_4 (0.28 T), P_5 (0.46 T), and P_6 (0.53 T). For example, the P_3 crossing leads to an interchange from a [Cu(↑)Dy(↓)Dy(↓)Cu(↑)] state to a [Cu(↓)Dy(↑)Dy(↓)Cu(↑)] state with a certain probability. Four dM/dB peaks appeared at 0.06, 0.12, approximately 0.19, and approximately 0.26 T. Some of them depended on the field-sweeping rate. In the adiabatic limit, the peak positions should be independent of the sweeping rate. This dependence on the sweeping rate might be ascribed to the nonadiabatic feature arising from very fast sweeping or mixing of residual thermal relaxation.[45] The number of the level crossing points and their positions are not so different from the theoretical prediction. The

(44) (a) Shklyaev, A. A.; Anufrienko, V. F.; Ogorodnikov, V. D. *Zh. Strukt. Khim.* **1973**, *14*, 994. (b) Hathaway, B. J.; Tomlinson, A. A. G. *Coord. Chem. Rev.* **1970**, *5*, 1.

(45) (a) Landau, L. *Phys. Z. Sowjetunion* **1932**, *2*, 46. (b) Zener, C. *Proc. R. Soc. London, Ser. A* **1932**, *137*, 696. (c) Stukelberg, E. C. G. *Helv. Phys. Acta* **1932**, *5*, 369.

deviation may be caused by some small perturbation such as intermacrocycle coupling *j* or dipolar interaction. On the other hand, the level structure determined by P_1 and P_2 is not affected by such perturbations.

In the present model, level crossings are classified into two regimes. The first group involves those at higher fields such as P_1 and P_2. The other group includes those at lower fields. This characteristic feature can be regarded as a fingerprint of the Ising type model for heterometallic molecular magnets including lanthanide ions, in sharp contrast to the nearly equally spaced steps in SMMs such as $[Mn_{12}]$[46] and $[Fe_{10}]$.[47] Since the Dy ions bring about very strong magnetic anisotropy and weak exchange couplings, we are informed by the level crossing fields on the magnitude of exchange couplings. On the other hand, the level crossings in 3d-based SMMs are regulated by the zero-field splitting parameter *D* and not *J*, because the *D* values are much smaller than the intramolecular *J*. We can regard the present Dy−Cu-based magnets, $[Dy_2Cu_2]_n$, as well as [DyCuDy][6] and $[Dy_4Cu]$,[7] as a new class of SMMs and SCMs, whose QTMs are based on a completely different principle.

Summary

The magnetic studies on $[Dy_2Cu_2]_n$ clarified the slow magnetization orientation and magnetization steps usually related to a SMM and SCM. We have reported here the precise evaluation of exchange coupling and energy levels by using a HF-EPR technique. To the best of our knowledge, the present work is the first example on determination of 4f−3d exchange parameters by means of EPR. By combining the magnetization and EPR results, we can precisely determine the exchange couplings in $[Dy_2Cu_2]_n$. The magnetic behavior of polymer $[Dy_2Cu_2]_n$ can be explained as a perturbed system of the monomeric SMM model $[CuDy_2Cu]$. The introduction of intermolecular interaction has been discussed for a dimer of the $[Mn_4]$-based SMM[48] and polymers of the $[Mn_2Ni]$-based SMMs.[49] We are now investigating the advantage of magnetically correlated SMMs compared with isolated SMMs in the Dy−Cu system.

The mechanism for the magnetization steps is quite different from that of the 3d-based SMMs;[1–3] the magnetization reorientation occurs through the internal flip of the elemental spins one by one, which finally brings about the reorientation as a whole. To exploit novel SMMs and SCMs showing such QTM, the present synthetic and EPR-analytic methodologies can be applied for isomorphic compounds of $[Dy_2Cu_2]_n$ and other Dy−Cu-based SMMs with replacing 4f and 3d metal ions. We believe that this work will lead to further designed magnets and functional magnetic materials.

Acknowledgment. This work was partly supported by Grants-in-Aid for Scientific Research from the Ministry of Education, Culture, Sports, Science and Technology, Japan (Nos. 15073101, 17550166, 18654058, and 19550135) and the Inter-University Cooperative Research Program of the Institute for Materials Research, Tohoku University.

Supporting Information Available: CIF file including selected geometrical parameter tables for $[Dy_2Cu_2]_n$. This material is available free of charge via the Internet at http://pubs.acs.org.

CM703530N

(46) Thomas, L.; Lionti, F.; Ballou, R.; Gatteschi, D.; Sessoli, R.; Barbara, B. *Nature* **1996**, *383*, 145.
(47) Wernsdorfer, W.; Ohm, T.; Sangregorio, C.; Sessoli, R.; Mailly, D.; Paulsen, C. *Phys. Rev. Lett.* **1999**, *82*, 3903.
(48) Wernsdorfer, W.; Aliaga-Alcalde, N.; Hendrickson, D. N.; Christou, G. *Nature* **2002**, *416*, 406.
(49) (a) Ferbinteanu, M.; Miyasaka, H.; Wernsdorfer, W.; Nakata, K.; Sugiura, K.; Yamashita, M.; Coulon, C.; Clérac, R. *J. Am. Chem. Soc.* **2005**, *127*, 3090. (b) Miyasaka, H.; Nezu, T.; Sugimoto, K.; Sugiura, K.; Yamashita, M.; Clérac, R. *Chem. Eur. J.* **2005**, *11*, 1592.